PERGAMON

International Journal of Solids and Structures 38 (2001) 7079–7100

INTERNATIONAL JOURNAL OF SOLIDS and STRUCTURES

www.elsevier.com/locate/ijsolstr

Similarity properties of demineralization and degradation of cracked porous materials

M. Mainguy, F.-J. Ulm *, F.H. Heukamp

Department of Civil and Environmental Engineering, Massachusetts Institute of Technology, Building 1-280, 77 Massachusetts Avenue, Cambridge, MA 02139-4307, USA

Received 7 August 2000

Abstract

The paper analyze the similarity properties of demineralization processes in cracked porous materials, coupled with diffusive and advective mass transfer through fractures. The aim is to find out, whether, when and how fractures accelerate or magnify the overall chemical degradation process. A dimensional analysis of a simplified dissolution process around a fracture channel reveals different self-similar properties for diffusion and advection dominated mass transport in the fracture. For a pure diffusive transport, the fracture degradation length develops with the quadratic root of time; while it evolves with the square root of time when advection dominates. These asymptotic behaviors are confirmed by model-based simulations of 'real' calcium leaching in cracked cement-based materials. It is shown, that a diffusion dominated mass transport in a fracture does not significantly accelerate the overall chemical degradation, since the one-dimensional-degradation through the porous material catches up with the initially faster diffusion through the fracture. In turn, advection dominated mass transfer in fractures can significantly accelerate the overall calcium depletion for 'high' fluid velocities in the fracture. Finally, diffusive dominated mass transport in a crack network may also accelerate the calcium leaching process for small values of crack spacing factors. A rough analytical solution for estimating this effect of a crack network is derived and validated through model-based simulations.

Keywords: Cracked porous media; Diffusion; Advection; Dissolution; Demineralization; Similarity properties; Asymptotic behavior; Durability; Fracture channel; Crack network; Model-based simulation

1. Introduction

It has long been argued, that cracks and fractures affect the durability of e.g. concrete structures subjected to chloride penetration, drying, calcium leaching, etc., due to the acceleration of the overall mass transport of liquids and ions through the crack network. However, less is known whether, when and how

* Corresponding author. Tel.: +1-617-253-3544; fax: +1-617-253-6044.
E-mail address: ulm@mit.edu (F.-J. Ulm).

0020-7683/01/$ - see front matter
PII: S0020-7683(00)00417-0

fractures accelerate or magnify the degradation process. For instance, in the case of chloride induced steel corrosion, Pettersson et al. (1996) and Schiessl and Raupach (1997) provided experimental evidence that small cracks do not significantly increase the risk of steel corrosion. On the other hand, studies reported by Samaha and Hover (1992) and Gérard and Marchand (2000) indicate that the material diffusivity may increase by up to 10–20%. Experimental results of Locoge et al. (1992) show that microcracks have no influence on the mass transfer as such, but can increase the amount of free chloride ions accessible to transfer. The effect of cracks on the moisture transport properties of cement based materials has also been studied. It has been found that cracks have a strong influence on the imbibition process in mortar and concrete (see Keer et al., 1989; Daïan and Saliba, 1993). Theoretical works have also pointed out that cracks may increase by several orders of magnitude the drying diffusivity of concrete (see e.g. Bažant and Raftshol, 1982). However, later experimental results revealed that cracks have a smaller influence on the drying process than theoretically expected (Bažant et al., 1987; Daïan and Saliba, 1993).

Cracks and fractures in concretes and rocks are critical to the durability performance of nuclear waste storage systems, as the safety of e.g. a deep geological nuclear waste disposal depends on the quality of both the host rock surrounding the repository (quantified by its low permeability), and the concrete barrier, liner and concrete encasement of containers. On the 'rock side', the effect of a fracture on the radionuclide transport in rock was subjected to intensive research (see e.g. Grisak and Pickens, 1980). It was found that the risk of water pollution by convective contaminant transport in rock fractures is reduced by diffusive losses in the matrix, since the porous material surrounding the crack (i.e. the host rock) may play the role of a diffusive sink (see e.g. Neretnieks, 1980; Tang et al., 1981). In addition, hyperalkaline fluid bordering the nuclear waste repository may deposit calcium in cracks and fractures of the surrounding rock (Savage and Rochelle, 1993; Steefel and Lichtner, 1994). On the 'concrete side', the problem of chemical degradation by calcium leaching induced by raining water or streaming water (for underground repositories) has been addressed in recent years. On a material level, the physical chemistry of chemical degradation due to water intrusion or streaming ground water is now well understood (see e.g. Berner, 1992; Reardon, 1992); and the chemical degradation of uncracked concrete over extended periods of time can be predicted today with some confidence by model-based simulations of the coupled diffusion–dissolution process (see e.g. Buil et al., 1992; Adenot, 1992; Adenot and Buil, 1992; Gérard, 1996; Delagrave et al., 1997; Torrenti et al., 1999; Ulm et al., 1999; Mainguy and Coussy, 2000; Mainguy et al., 2000). The effect of a fracture or a crack network, however, on the overall chemical degradation process of concrete structures, which may ultimately impair the shielding function of the concrete barrier, is still not clear (Gérard, 1996; Tognazzi, 1998). Current practice in concrete application in nuclear waste containment is to accept or reject a concrete container with regard to crack size specifications.

The purpose of this paper, therefore, is to analyze the effect of cracks and fractures on coupled diffusion–dissolution processes in porous materials. While developed around the topic of the demineralization process of cementitious materials, this analysis may also be relevant to other diffusion–dissolution, diffusion–sorption, and diffusion–precipitation processes that occur in cracked porous materials, ranging from thermal oxidation of silicon during manufacturing of integrated circuits (Rao and Hughes, 2000), oxidation of titanium alloys (Lagoudas et al., 2000) to the demineralization of trabecular bone leading to osteoporosis (Martin and Burr, 1989). The paper is organized as follows: In the first part, we will investigate the similarity properties of an idealized coupled diffusion–dissolution process in a porous material separated by a fracture channel, through which dissolved ions are transported by both diffusion and advection. The similarity properties will be analyzed in the second part of this paper by numerical simulations of 'real-life' multi-stage demineralization processes, which characterize calcium leaching in cement-based materials. Finally, the problem of a crack network constituted of equally spaced parallel fractures of same width will be addressed. Some practical conclusions as for the durability performance of concrete affected by cracks will be drawn at the end of this paper.

2. Reference problem: diffusion and advection in a fracture channel of a chemically reactive porous medium

2.1. Idealized geometry and problem

Consider a semi-infinite porous medium $y > 0$, separated at $x = 0$ by a semi-infinite fracture channel of constant width $2b$ (Fig. 1). The porous continuum is assumed to be composed of a solid skeleton, in which a mineral (e.g. calcium) is bound, which is also present in ionic form (e.g. Ca^{2+}-ions) in the interstitial pore solution saturating the pore space. Initially at chemical equilibrium, a demineralization process (e.g. calcium depletion) will occur when the ionic mineral concentration in the interstitial solution is lowered through a prescribed mineral concentration at the boundary, which is lower than the equilibrium calcium concentration. For the simplified problem at hand, this boundary is composed of the boundary of the porous material, $x \notin]-2b; 0[$, and the fracture channel walls $y > 0$ at $x = 0$ and $x = -2b$. It is through this fracture channel, that calcium can be evacuated at a higher diffusion rate (when compared to the diffusivity of the porous material). It is usually assumed that the ion transport through the fracture is governed by pure diffusion. Recent experimental results of calcium leaching of cracked cementitious materials, however, suggest that calcium in the fracture may also be transported by water flux, evacuating at 'high' velocity of the solvent (e.g. water) the solute through the fracture (Torrenti et al., 1999). In deed, cement-based materials are low permeable porous media where water flow is usually a slow process. Hence, the hydraulic conductivity of an individual fracture is large in comparison with the low hydraulic material conductivity, such that a small crack in a large concrete slab may dominate the flow system (Walton and Seitz, 1992). This motivates the study of both diffusion dominated and advection dominated mass transport in the fracture.

To study the similarity properties of the simplified problem, the following assumptions are introduced:

(1) The fracture width $2b$ and the porosity ϕ of the solid matrix are not changed due to the mineral dissolution process. The diffusion coefficient in the solid matrix D_m and the hydrodynamic coefficient in the fracture D_f, therefore, will be assumed constant. In addition, the idealized geometry of smooth and parallel

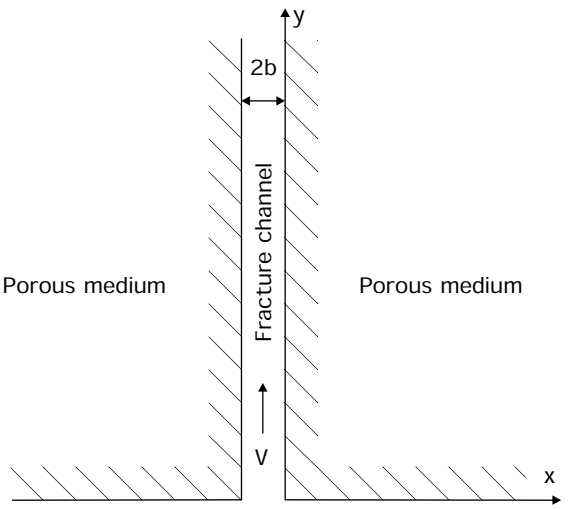

Fig. 1. Fracture–porous medium system. A diffusion/advection process occurs in the fracture coupled with diffusion and dissolution in the porous medium.

fracture walls comes to assume tortuosity effects negligible, and corresponds to an upper bound of the flow that occurs in 'real' non-smooth fractures encountered in cement-based materials.

(2) The fracture opening, $2b$, is much smaller than the fracture length; and the concentration in x-direction in the fracture has a uniform value at all times. Furthermore, the flow of the solvent in the fracture is assumed laminar with average velocity V representing the simplest case of a constant hydraulic gradient along the fracture. These hypotheses provide the basis for a one-dimensional (1D) analysis of mass transport along the fracture (Tang et al., 1981).

(3) The diffusion process in the matrix only occurs in the x-direction (i.e. no diffusion in the y-direction), and is driven by a zero solute concentration boundary condition prescribed at the inlet of the channel at $y = 0$ over the fracture width $-2b < x < 0$. This comes to assume a much faster diffusion or advection process in the fracture than in the adjacent porous material.

2.2. Governing equations

In the simplified model, it is assumed that the ions, which are dissolved in the uncracked material, are only evacuated through the fracture. The corresponding mass conservation in the x-direction in the porous material reads (Bear, 1991; Mainguy and Coussy, 2000):

$$\phi \frac{\partial \rho_{\mathrm{m}}}{\partial t} + \frac{\partial m_{\mathrm{m}}}{\partial t} - \frac{\partial}{\partial x}\left(\phi D_{\mathrm{m}} \frac{\partial \rho_{\mathrm{m}}}{\partial x}\right) = 0, \quad x, y, t > 0. \tag{1}$$

and the one in the fracture (Bear, 1993):

$$\frac{\partial \rho_{\mathrm{f}}}{\partial t} + \frac{\partial}{\partial y}\left(-D_{\mathrm{f}} \frac{\partial \rho_{\mathrm{f}}}{\partial y} + V \rho_{\mathrm{f}}\right) + \frac{[q_x]}{2b} = 0, \quad y, t > 0. \tag{2}$$

In Eqs. (1) and (2), $\rho_{\mathrm{m}} = \mathscr{M} c$ and $\rho_{\mathrm{f}} = \mathscr{M} c$ denote the concentration of the solute (e.g. calcium ions), with $\mathscr{M}$ the molar mass of the solute, and c the molar concentration. In Eq. (1), m_{m} stands for the apparent volume mass of the same mineral bound in the skeleton, and $\partial m_{\mathrm{m}}/\partial t$ is the skeleton mass variation due to the dissolution process described below. The solvent in the porous continuum is assumed at rest, so that the solute mass transport only occurs through molecular diffusion, described by Fick's first law (term of the form $-\phi D_{\mathrm{m}} \partial \rho_{\mathrm{m}}/\partial x$). In turn, the ion flux in the fracture in Eq. (2) is governed by two phenomena: The flux $-D_{\mathrm{f}} \partial \rho_{\mathrm{f}}/\partial y$ accounts for the diffusive mass transport in the fracture and the mechanical dispersion originating from variations of the fluid velocity across the fracture (i.e., Taylor (1953) dispersion) and the roughness of the fracture wall (see e.g. Ippolito et al., 1994; Sun, 1996). However, due to the assumed perfect geometry of the fracture, this geometrical dispersion will not be considered in this study. The second phenomenon is the ion flux transported by advection of the solvent (e.g. water) at velocity V through the fracture, and is expressed by $V \rho_{\mathrm{f}}$ in Eq. (2). Finally, $[q_x]$ stands for the jump in solute flux over the fracture of opening $2b$. This jump can be expressed from the diffusive flux associated with Fick's first law from the adjacent porous continuum at $x = 0$. Taken the symmetry of the fracture channel, this jump is equal to twice the diffusive flux from the adjacent porous material:

$$[q_x] = -2\phi D_{\mathrm{m}} \frac{\partial \rho_{\mathrm{m}}}{\partial x}|_{x=0}. \tag{3}$$

The mass conservation and conduction laws need to be completed by the chemical dissolution law and the initial and boundary conditions. At chemical equilibrium, the molar concentration c of the solute in the interstitial pore solution is equal to the chemical equilibrium concentration c_{eq}. Chemical equilibrium means that the probability that the mineral will dissolve from the skeleton is equal to the probability that another molecule will precipitate from the solution onto the skeleton. In return, if $c < c_{\mathrm{eq}}$, the mineral will dissolve from the skeleton. If we note $\rho_{\mathrm{eq}} = \mathscr{M} c_{\mathrm{eq}}$ the corresponding volume mass density at chemical

equilibrium, and m_m the apparent volume mass of the same mineral bound in the skeleton, the instantaneous dissolution of the mineral bound in the skeleton is described by (Mainguy and Coussy, 2000):

$$m_m \geqslant 0; \qquad \rho_m - \rho_{eq} \leqslant 0; \qquad m_m(\rho_m - \rho_{eq}) = 0. \tag{4}$$

Furthermore, at the interface $x = 0$ between the fracture and the matrix, the continuity of the solute concentration c reads:

$$\rho_f(y,t) = \rho_m(0,y,t), \quad y, t > 0. \tag{5}$$

In addition, for an initially undegraded material, the initial conditions at time $t = 0$ are defined by Eq. (4):

$$\rho_m(x,y,0) = \rho_{eq}, \qquad m_m(x,y,0) = m_0, \quad x, y > 0, \tag{6}$$

where m_0 is the initial apparent volume mass density of the mineral bound in the skeleton. Eqs. (5) and (6) define the initial condition in the fracture:

$$\rho_f(y,0) = \rho_m(0,y,0) = \rho_{eq}, \quad y \geqslant 0. \tag{7}$$

and the boundary condition reads:

$$\rho_f(y=0,t) = 0, \quad t > 0. \tag{8}$$

It is remarkable that the problem defined by the set of equations (1) to (8) simplifies to two orthogonal 1D diffusion problems coupled through the concentration continuity at the interface $x = 0$, and the influx of solute from the porous medium into the fracture channel. The boundary condition (8) at the inlet of the fracture will induce a decrease of solute concentration in the fracture through diffusion and advection. Then the coupling between the two 1D equations through Eq. (5) will lead to a decrease of the solute concentration in the porous continuum. In turn, the solute flux (3) will trigger a dissolution process in the x-direction, inducing a chemical degradation of the porous material.

2.3. Invariants of diffusion or advection dominated flow in the fracture

A preliminary screening of invariants of the problem defined by the set of equations (1) to (8) indicates that the dimensionless unknowns of the problem,

$$\bar{\rho}_f = \frac{\rho_f}{\rho_{eq}}; \qquad \bar{\rho}_m = \frac{\rho_m}{\rho_{eq}}; \qquad \bar{m}_m = \frac{m_m}{m_0} \tag{9}$$

are functions of the following five invariants:

$$\pi_1 = \frac{x}{2\sqrt{D_m t}}; \quad \pi_2 = \frac{y}{2\sqrt{D_f t}}; \quad \pi_3 = \frac{y}{Vt}; \quad \pi_4 = \frac{\sqrt{D_m t}}{b/\phi}; \quad \pi_5 = \frac{\phi\rho_{eq}}{m_0}. \tag{10}$$

Invariants π_1 and π_2 are the Boltzmann variables of the two 1D diffusion problems in the porous continuum and the fracture considered separately. In turn, following first principles of dimensional analysis, a combination of invariants π_2 and π_3 gives the following invariant

$$\overline{Pe} = 4\frac{\pi_2^2}{\pi_3} = \frac{Vy}{D_f}. \tag{11}$$

For a characteristic length scale $y \equiv L_y$ of the diffusion or advection in the fracture, this invariant turns out to be the Péclet number $Pe = VL_y/D_f$, which quantifies the relative importance of the diffusive transport versus the advective transport of solute through the fracture: for $Pe \ll 1$, the effect of advection becomes negligible compared to the diffusion process, and the problem is governed by a pure diffusive mass transfer in the fracture; and for $Pe \gg 1$ it is the inverse. The remaining invariants π_4 and π_5 will be detailed later.

It is instructive to inspect the solution of the problem in terms of the invariants governing the two limit cases of a diffusion dominated and an advection dominated mass transport in the fracture:

• For $Pe \ll 1$, the solution does not depend on π_3, and the unknowns of the problem (9) depend only on invariants π_1, π_2, π_4 and π_5:

$$\bar{\rho}_f = \mathscr{F}(\pi_2, \pi_4, \pi_5); \qquad \bar{\rho}_m = \mathscr{G}(\pi_1, \pi_2, \pi_4, \pi_5); \qquad \bar{m}_m = \mathscr{H}(\pi_1, \pi_2, \pi_4, \pi_5) \tag{12}$$

or equivalently:

$$\bar{\rho}_f = \mathscr{F}(\bar{y}, \bar{t}, \varepsilon); \qquad \bar{\rho}_m = \mathscr{G}(\bar{x}, \bar{y}, \bar{t}, \varepsilon); \qquad \bar{m}_m = \mathscr{H}(\bar{x}, \bar{y}, \bar{t}, \varepsilon), \tag{13}$$

where we made use of the assumption of a uniform distribution in the x-direction of the solvent in the fracture. In Eq. (13), $\bar{x} = \pi_1$, $\bar{t} = \pi_4$, $\varepsilon = \pi_5$, while the dimensionless coordinate $\bar{y}$ characterizing the diffusion process in the fracture is obtained as product and power function of the invariants π_2 and π_4:

$$Pe \ll 1: \quad \bar{y} = \pi_2\sqrt{2\pi_4} = y\sqrt{\frac{1}{D_f(2b/\phi)}}\left(\frac{D_m}{t}\right)^{1/4}. \tag{14}$$

• For $Pe \gg 1$, the second invariant π_2 does not enter the solution of the problem, i.e.:

$$\bar{\rho}_f = \mathscr{F}(\pi_3, \pi_4, \pi_5); \qquad \bar{\rho}_m = \mathscr{G}(\pi_1, \pi_3, \pi_4, \pi_5); \qquad \bar{m}_m = \mathscr{H}(\pi_1, \pi_3, \pi_4, \pi_5) \tag{15}$$

or equivalently:

$$\bar{\rho}_f = \mathscr{F}(\bar{y}, \bar{t}, \varepsilon); \qquad \bar{\rho}_m = \mathscr{G}(\bar{x}, \bar{y}, \bar{t}, \varepsilon); \qquad \bar{m}_m = \mathscr{H}(\bar{x}, \bar{y}, \bar{t}, \varepsilon) \tag{16}$$

where the dimensionless coordinate $\bar{y}$ characterizing the advection process in the fracture is now obtained as a product function of the invariants π_3 and π_4:

$$Pe \gg 1: \quad \bar{y} = \frac{\pi_3\pi_4}{2} = \frac{y}{V(2b/\phi)}\left(\frac{D_m}{t}\right)^{1/2}. \tag{17}$$

Eqs. (14) and (17) indicate a self-similar time–space relation proportional to the quadratic root of time in a diffusion controlled mass transport in the fracture (i.e., $y(t) \propto t^{1/4}$ if $Pe \ll 1$), and a square root dependency for an advection controlled mass transport (i.e., $y(t) \propto t^{1/2}$ if $Pe \gg 1$). The $t^{1/4}$-dependency of the diffusion controlled mass transport translates the fact that the mass transport is governed by two coupled 1D-diffusion process, one in the y-direction through the fracture, the other in the x-direction through the bulk material. In return, the advection dominated mass transport through the fracture is governed by a given solvent velocity V, and the rate-determining process, therefore, is defined by the $t^{1/2}$-dependency of the solute arrival in the fracture.

Finally, the remaining invariants $\bar{x} = \pi_1$, $\bar{t} = \pi_4$ and $\varepsilon = \pi_5$ are not affected by the mass transport mode in the fracture. This is readily understood from their physical significance: Invariant $\bar{x} = \pi_1$ is the Boltzmann variable characterizing the diffusion process in the porous material, which is not affected by the transport mode in the fracture. Similarly, the invariant $\bar{t} = \pi_4$ is a normalized time invariant, which relates the solute diffusion length $2\sqrt{D_m t}$ in the porous material to the fracture width, or more precisely to an effective fracture width, magnified by the inverse of the bulk porosity, $2b/\phi$. This invariant introduces a gauge time τ_b, which is not changed when the Péclet number changes:

$$\bar{t} = \pi_4 = \left(\frac{t}{\tau_b}\right)^{1/2}; \qquad \tau_b = \frac{(b/\phi)^2}{D_m}. \tag{18}$$

Last, invariant $\varepsilon = \pi_5$ can be interpreted as a macroscopic solubility constant of the dissolution process, which relates at equilibrium the apparent chemical equilibrium mineral mass density in solution, $\phi\rho_{eq}$, to the initial mineral mass density, m_0, in the solid phase:

$$\varepsilon = \pi_5 = \frac{\phi \rho_{\mathrm{eq}}}{m_0}. \tag{19}$$

With these invariants in hand, it becomes possible to study the asymptotic behavior of diffusion dominated and advection dominated mass transport in the fracture.

2.4. Large time asymptotic behavior of diffusion and advection dominated flow in the fracture

We first recall the solution of the 1D problem of diffusion and dissolution in the porous medium. This problem is obtained when solving the set of equations (1) and (4) for $y = 0$ and $x > 0$, together with a zero boundary condition prescribed at $x = 0$. This problem is similar to the well-known Stefan Problem often encountered in heat problems with change of state (see e.g. Carslaw and Jaeger, 1959). In the considered case of an instantaneous demineralization process, the solution is characterized by the presence of a sharp dissolution front or wave (Lichtner et al., 1986; Novak, 1993) propagating at finite velocity through the bulk material. The position x_{d} of the dissolution front depends on the square root of time, and is given by (Mainguy and Coussy, 2000):

$$x_{\mathrm{d}}(t) = 2\bar{x}_{\mathrm{d}}(\varepsilon)\sqrt{D_{\mathrm{m}} t}, \tag{20}$$

where $\bar{x}_{\mathrm{d}} = \bar{x}_{\mathrm{d}}(\varepsilon)$ is the solution of the following equation:

$$\varepsilon \exp(-\bar{x}_{\mathrm{d}}^2) - \sqrt{\pi}\bar{x}_{\mathrm{d}} \mathrm{erf}(\bar{x}_{\mathrm{d}}) = 0. \tag{21}$$

The dissolution front located by x_{d} (see Fig. 2) separates a completely degraded zone where the solid mineral is entirely dissolved ($m_{\mathrm{m}} = 0$ for $x < x_{\mathrm{d}}$), from an undegraded zone where the solid mineral is at the initial value ($m_{\mathrm{m}} = m_0$ for $x > x_{\mathrm{d}}$).

The instantaneous dissolution process implies also the existence of a finite degraded depth along y at the fracture–solid matrix interface ($x = 0$). This degraded depth, to which we will refer as fracture degradation length, is noted y_{d} and is shown in Fig. 2. For large times $\bar{t} \gg 1 \leftrightarrow t \gg \tau_{\mathrm{b}}$, for which the mass transport in the fracture is in a quasi-steady state condition with the solute influx from the surrounding porous medium,

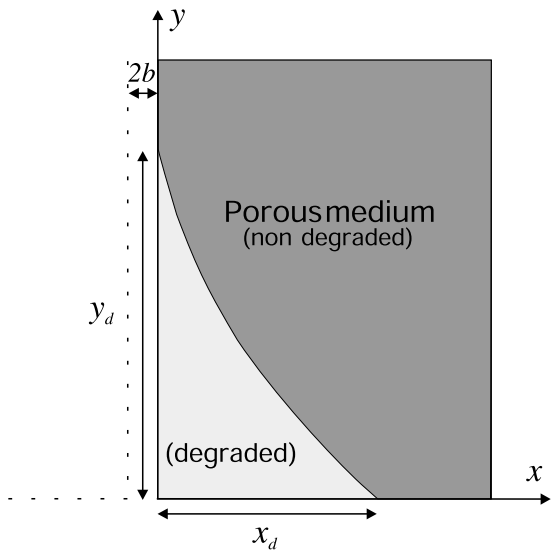

Fig. 2. Definition of the degradation profile with x_{d} and y_{d} the degradation lengths in the x-direction and along the fracture channel.

the solution of the problem becomes independent of the normalized time $\bar{t}$, and Eqs. (13) and (16) reduce to (Mainguy and Ulm, 2000):

$$\bar{\rho}_{\mathrm{f}} = \mathscr{F}(\bar{y}, \varepsilon); \quad \bar{\rho}_{\mathrm{m}} = \mathscr{G}(\bar{x}, \bar{y}, \varepsilon); \quad \bar{m}_{\mathrm{m}} = \mathscr{H}(\bar{x}, \bar{y}, \varepsilon). \tag{22}$$

In Eq. (22), $\bar{y}$ depends on the Péclet number. More precisely, Eqs. (14), (17) and (22) imply the following forms of y_{d} for the two limit cases at large times:

- Diffusion dominated $Pe \ll 1$:

$$t \gg \tau_{\mathrm{b}}: \quad y_{\mathrm{d}}^{\mathrm{dif}}(t) = \bar{y}_{\mathrm{d}}^{\mathrm{dif}}(\varepsilon)\sqrt{D_{\mathrm{f}}\frac{2b}{\phi}}\left(\frac{t}{D_{\mathrm{m}}}\right)^{1/4}, \tag{23}$$

where $\bar{y}_{\mathrm{d}}^{\mathrm{dif}}(\varepsilon)$ is the dimensionless front position function, which – similarly to $\bar{x}_{\mathrm{d}}(\varepsilon)$ in Eq. (20) – links the fracture degradation length to the macroscopic solubility ε. Eq. (23) indicates that the fracture degradation length develops as a linear function of the quadratic root of time ($y_{\mathrm{d}}^{\mathrm{dif}} \propto t^{1/4}$), and is scaled by the square root of the crack opening ($y_{\mathrm{d}}^{\mathrm{dif}} \propto \sqrt{2b/\phi}$). For large times $t \gg \tau_{\mathrm{b}}$, due to the $t^{1/4}$-dependency, the diffusion through the fracture slows down in time, in comparison with the 1D degradation process, which penetrates with the square root of time into the uncracked bulk material. The solute diffusion through the fracture, therefore, is not expected to significantly increase the chemical degradation of the material.

- Advection dominated $Pe \gg 1$:

$$t \gg \tau_{\mathrm{b}}: \quad y_{\mathrm{d}}^{\mathrm{adv}}(t) = \bar{y}_{\mathrm{d}}^{\mathrm{adv}}(\varepsilon) V \frac{2b}{\phi}\left(\frac{t}{D_{\mathrm{m}}}\right)^{1/2}, \tag{24}$$

where $\bar{y}_{\mathrm{d}}^{\mathrm{adv}}(\varepsilon)$ is the dimensionless front position function of the advection dominated transport mode in the fracture. The fracture degradation length evolves here as a function of the square root of time ($y_{\mathrm{d}}^{\mathrm{adv}} \propto t^{1/2}$), and is scaled linearly by the crack opening ($y_{\mathrm{d}}^{\mathrm{adv}} \propto 2b/\phi$). A $t^{1/2}$-dependency also characterizes the degradation process in the uncracked porous material (i.e. Eq. (20)). Hence, it is expected that the advective transport of ions through the fracture may increase the overall degradation kinetics of the bulk material by a multiplying factor, depending on the solvent velocity V and the effective crack opening $2b/\phi$.

In between these two limit cases, the evolution of the degraded depth along the fracture cannot be determined analytically. However, as the Péclet number goes from small values to large values, it can be expected, that the degraded depth development will switch progressively from the asymptotic quadratic root behavior in time to a square root behavior.

3. Similarity properties of 'real' calcium leaching in cracked cement-based materials

The relevance of the asymptotic solutions (23) and (24) of the studied reference problem is defined by the gauge time τ_{b}, which increases with $(b/\phi)^2/D_{\mathrm{m}}$. For concrete applications in nuclear waste containment, maximum crack openings due to shrinkage are on the order of $2b \leqslant 1$ mm, the porosity is on the order of $\phi = 0.1$–0.5, and the calcium diffusivity is $\phi D_{\mathrm{m}} \approx 10^{-12}$–$10^{-11}$ m^2/s (Tognazzi, 1998). This gives a rough estimate of $\tau_{\mathrm{b}} \leqslant 30$ days, which implies that the asymptotic expressions (23) and (24) are relevant for assessing the effect of cracks on the chemical degradation process of concrete at the time-scale of nuclear waste disposal of 300–1000 years. This motivates the analysis of the similarity properties of 'real' calcium leaching in cracked porous cement-based materials, the reference scenario of design and operation of safe nuclear waste underground storage systems. 'Real' calcium leaching in cement-based materials is a multi-stage process, which involves the successive demineralization of different constituents of the mineral matrix

at specific calcium ion concentrations in the interstitial pore solution (see e.g. Berner, 1988, 1992; Adenot, 1992; Reardon, 1992). This leads to multiple dissolution fronts and an increase in porosity ϕ, which were not considered in the 1D single phase demineralization process analyzed before. The non-linearity of the process requires numerical simulations.

3.1. Model, model parameters and finite element implementation of calcium leaching in cracked cement-based materials

The model we consider is a two-dimensional (2D) extension of the 1D diffusion models, given by Eqs. (1)–(4). The coupled diffusion–dissolution process in the uncracked cement-based material is described by the molar mass balance equation:

$$\frac{\partial}{\partial t}(\phi c) + \frac{\partial s}{\partial t} - \nabla \cdot (\mathbf{D}_{\text{eff}} \cdot \nabla c) = 0 \tag{25}$$

and a chemical equilibrium condition of the multi-stage dissolution process:

$$s - g(c) = 0. \tag{26}$$

In (25), $c = \rho_m/\mathscr{M}$ is the molar concentration of the calcium in the interstitial pore solution. It is related through the chemical equilibrium condition (26), which replaces (4), to the molar concentration of calcium, $s = m_{\text{m}}/\mathscr{M}$, bound in the different minerals of the solid matrix. $\mathbf{D}_{\text{eff}}$ is the tensor of effective ion diffusivities of calcium in the porous material, and depends on the porosity ϕ, which in turn depends on the solid concentration, and thus on the solid molar concentration s. Functions $\mathbf{D}_{\text{eff}} = D_{\text{eff}}(\phi)\mathbf{1}$ ($\mathbf{1}$ = second-order unit tensor), $\phi = \phi(s)$ and the chemical equilibrium condition (26) are fully described in Mainguy et al. (2000) for a cement paste of water:cement ratio equal to w/c = 0.4.

Analogously, the mass balance in the fracture is written in molar form:

$$\frac{\partial c}{\partial t} - \nabla \cdot (\mathbf{D}_{\text{f}} \cdot \nabla c + \mathbf{V} c) = 0. \tag{27}$$

In contrast to the simplified 1D-model (i.e., Eq. (2)), the calcium influx (3) from the surrounding porous material need not to be considered explicitly, but is handled in the 2D-model through the continuity condition at the fracture–matrix interface. Furthermore, in Eq. (27), the average fluid velocity vector $\mathbf{V}$ of the solvent in the fracture is assumed to be oriented in the y-direction of the fracture, i.e. $\mathbf{V} = V\mathbf{e}_y$. The tensor of hydrodynamic dispersion coefficients in the fracture $\mathbf{D}_{\text{f}}$ accounts for the molecular diffusion in the fracture, but also for the fluid mechanical dispersion due to the transversal variations of the fluid velocity across the fracture ('Taylor' dispersion), even though molecular diffusion in concrete applications dominates over fluid dispersion. For the 2D-problem at hand, $\mathbf{D}_{\text{f}}$ is given in the form (Bear, 1991):

$$\mathbf{D}_{\text{f}} = D^*\mathbf{1} + \alpha_y V \mathbf{e}_y \otimes \mathbf{e}_y \tag{28}$$

with D^* the isotropic calcium diffusion coefficient in free water, and $\alpha_y V$ the longitudinal 'Taylor' dispersion coefficient. In the numerical investigation, the calcium diffusion coefficient is fixed at an upper bound value of $D^* = 2 \times 10^{-9}\ \text{m}^2\,\text{s}^{-1}$, and the Taylor dispersion coefficient is estimated from Aris (1956) solution:

$$\alpha_y V = \frac{(2b)^2 V^2}{210 D^*}. \tag{29}$$

Eqs. (25)–(29) are solved using the finite element method based on a variational formulation of the problem with s and c as principal unknowns, linked by the chemical equilibrium condition (26) at the fracture–matrix interface. In the uncracked matrix, the use of $s = s(\mathbf{x}, t)$ as principal unknown within low order finite elements (linear basis functions), together with an implicit time integration scheme and mass lumping (see, e.g. Hughes, 1987), ensures an accurate oscillation-free determination of the position of the

dissolution fronts in time and space. In the fracture, where the bound calcium concentration has no significance, the calcium concentration $c = c(\mathbf{x}, t)$ is employed as principal unknown. Finally, the continuity of both the calcium concentration and the normal calcium flux in the two-field discretization (s in the matrix, c in the fracture) is efficiently realized through the implementation of the chemical equilibrium condition (26) into two-node penalty elements with c_i as degree of freedom in the fracture, and s_i as degree of freedom on the matrix side. Last, space and time step increments are selected such to avoid the effects of numerical dispersion and overshoot, which may result from high fluid flow velocity in the fracture (see, for instance, Sun, 1996).

Taken the symmetry of the fracture channel and surrounding porous medium, the finite element simulations are realized on half of the geometry displayed on Fig. 1, with a zero flux boundary condition applied along the fracture center line (symmetry), and on the top and right sides of the rectangular geometry (far field conditions). Initial conditions correspond to a calcium molar solid concentration of $s(\mathbf{x}, t = 0) = 14.7 \times 10^3$ mol/m^3, which is related by chemical equilibrium (i.e., Eq. (26)) to an interstitial calcium concentration of $c(\mathbf{x}, t = 0) = 21$ mol/m^3 (Mainguy et al., 2000). Two degradation scenarios are studied in what follows, corresponding to different boundary conditions:

- $\mathscr{B}1$: A zero calcium concentration prescribed at the inlet of the fracture. This case corresponds precisely to the simplified 1D-degradation scenario, for which the similarity properties were previously derived. In this case, the solid material diffusivity in the y-direction is set to zero (i.e., $D^{yy}_{\text{eff}} = \mathbf{e}_y \cdot \mathbf{D}_{\text{eff}} \cdot \mathbf{e}_y = 0$), which implies a zero flux boundary condition along $y = 0$ and $x > b$ (Logan et al., 1998).
- $\mathscr{B}2$: A zero calcium concentration prescribed along $y = 0$ on both solid material and fracture inlet. This case corresponds to the realistic degradation process of cracked porous media, and will allow us to analyze the validity of asymptotic behaviors previously identified for the idealized degradation process. In this case, the solid material diffusivity is assumed isotropic, $\mathbf{D}_{\text{eff}} = D_{\text{eff}}\mathbf{1}$.

3.2. Pure diffusive mass transfer in the fracture

A first application of the model is concerned with the study of the effect of the fracture width for a pure diffusive mass transfer in the fracture ($Pe \equiv 0$). For boundary conditions $\mathscr{B}1$, Fig. 3 displays the evolution of the fracture degradation length $y_{\text{d}}^{\text{dif}}$ versus the quadratic square root of time $t^{1/4}$ for different fracture openings, ranging from $2b = 0.1$ mm to $2b = 1$ mm. Fig. 4 shows the same results, but in a plot of $y_{\text{d}}^{\text{dif}}/\sqrt{2b}$ versus $t^{1/4}$ for the maximum and minimum crack opening. Noting that $y_{\text{d}}^{\text{dif}}$ characterizes the position of the Portlandite dissolution front, which is the first mineral dissolved in cause of 'real' calcium depletion, the numerical results confirm the similarity properties of the asymptotic solution (23), i.e.:

- The asymptotic self-similarity $y_{\text{d}}^{\text{dif}} \propto t^{1/4}$, which is reached for large times $t \gtrsim 2$ years. This is consistent with the estimated gauge time $\tau_{\text{b}} \leqslant 30$ d fixed by the application (i.e., $t \gg \tau_{\text{b}}$).
- The $\sqrt{2b}$-magnification of the diffusion induced degradation process through the fracture, highlighted by a perfect alignment of the results along a straight-line in the $y_{\text{d}}^{\text{dif}}/\sqrt{2b} \times t^{1/4}$-plot, displayed in Fig. 4. By linear regression, the numerical results for $t \geqslant 2$ years can be expressed in the form of (23):

$$\frac{y_{\text{d}}^{\text{dif}}(t)}{\sqrt{2b}} = 1.73t^{1/4} - 0.84 \tag{30}$$

with $y_{\text{d}}^{\text{dif}}$ and $2b$ in cm, and time t in days.

The asymptotic solution (23), therefore, still holds despite the non-linearity of porosity $\phi = \phi(s)$, diffusivity $D_{\text{eff}} = D_{\text{eff}}(\phi)$, and chemical equilibrium condition $s = g(c)$, that characterize 'real' calcium leaching. It can be employed for assessing the Portlandite dissolution front, when replacing the diffusivity of

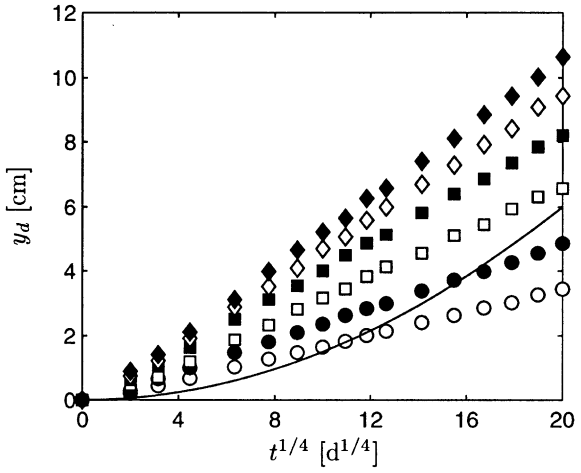

Fig. 3. Fracture degradation length y_d versus $t^{1/4}$ for a pure diffusive mass transport in the fracture, a zero solid matrix diffusivity in the y-direction and different crack openings $2b$: (○) 0.1 mm; (●) 0.2 mm; (□) 0.4 mm; (■) 0.6 mm; (◇) 0.8 mm; (♦) 1 mm. The solid line corresponds to the 1D degradation of the solid matrix ($x_d = 1.5 \times 10^{-2}\sqrt{t}$ with t in days and x_d in cm) (boundary condition $\mathscr{B}1$).

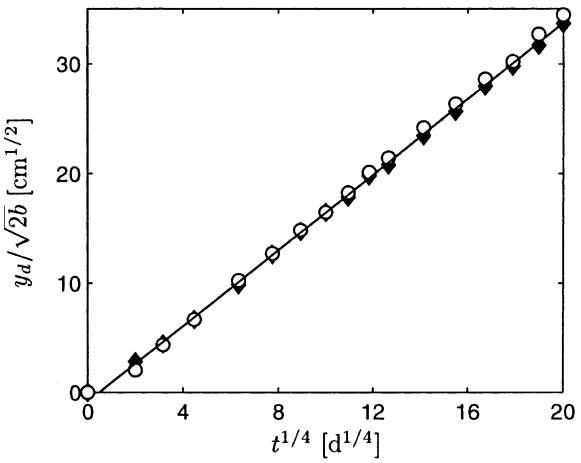

Fig. 4. Fracture degradation length $y_d/\sqrt{2b}$ versus $t^{1/4}$ for a pure diffusive mass transport in the fracture, and for different crack openings $2b$: (○) 0.1 mm and (♦) 1 mm. The solid line corresponds to the linear regression (30) of data for crack widths 0.1, 0.2, 0.4, 0.6, 0.8, and 1 mm, and times $t > 2$ years. (boundary condition $\mathscr{B}1$).

the solid matrix (D_m) and the porosity (ϕ) in Eq. (23) by the values of the same parameters of the undegraded material.

Finally, from a practical point of view, the confirmed asymptotic behavior suggests – for large times – an insignificant acceleration of the bulk material degradation through the diffusion dominated mass transfer in the fracture, in comparison with a 1D-dissolution process that originates from the boundary at $x = 0$. This is illustrated in Fig. 3, in which the solid line represents the front position of the 1D-dissolution process through the bulk material (similarly to Eq. (20)). As time flows, the 1D-degradation process, which evolves with the square root of time, reaches and overtakes the fracture degradation length $y_d^{dif}(t)$ evolving with the

quadratic root of time. This behavior is confirmed through a refined analysis applying boundary conditions $\mathscr{B}2$. The degraded depth $y_d^{dif}(t)/\sqrt{2b}$ versus $t^{1/4}$ is given in Fig. 5, and need to be compared with Fig. 4. We note a significant deviation from the asymptotic behavior (30) for times $t \geqslant 2$–10 years, depending on the crack opening. This deviation corresponds to the switch from the diffusion-induced degradation through the fracture ($y_d^{dif}(t) \propto t^{1/4}$), to the diffusion-induced degradation through the solid porous material ($y_d(t) \propto t^{1/2}$); and the time for this switch to occur corresponds to the time it takes the 1D-diffusion–dissolution process prevailing in the bulk material to reach the slower $t^{1/4}$-diffusion in the fracture. This switch can also be depicted from Fig. 6, which shows the same as Fig. 5, but now plotted as a function of the square root of

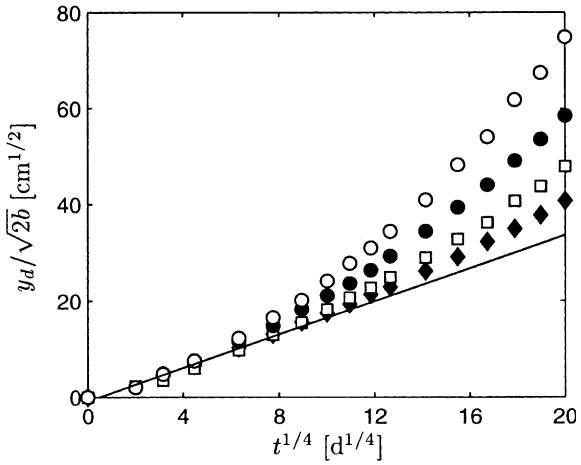

Fig. 5. Fracture degradation length $y_d/\sqrt{2b}$ versus $t^{1/4}$ for a pure diffusive mass transport in the fracture, isotropic solid matrix diffusivity, and different crack openings $2b$: (○) 0.1 mm; (●) 0.2 mm; (□) 0.4 mm; (■) 1 mm. The solid line corresponds to the linear regression (30) (boundary condition $\mathscr{B}2$).

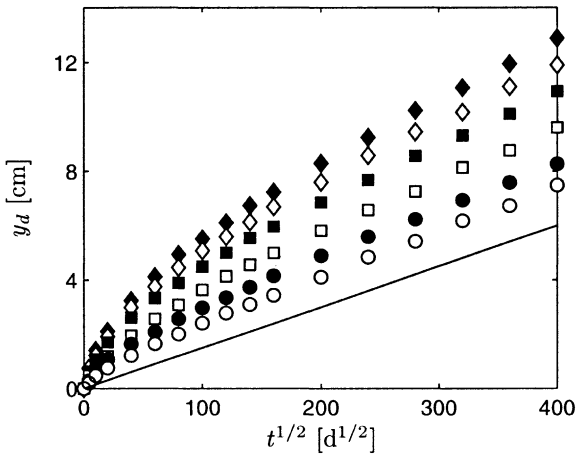

Fig. 6. Fracture degradation length y_d for a pure diffusive mass transport and different crack openings $2b$: (○) 0.1 mm; (●) 0.2 mm; (□) 0.4 mm; (■) 0.6 mm; (◇) 0.8 mm; (◆) 1 mm. The solid line corresponds to the 1D degradation of the solid matrix ($x_d = 1.5 \times 10^{-2}\sqrt{t}$ with t in days and x_d in cm) (boundary condition $\mathscr{B}2$).

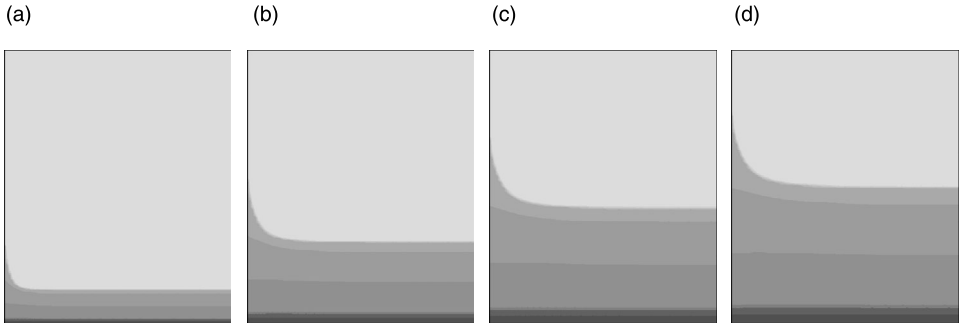

Fig. 7. Solid calcium concentrations for a pure diffusive mass transport in the fracture at different times. (Crack width $2b = 0.4$ mm, mesh $= 10 \times 12$ cm^2) (boundary condition $\mathscr{B}2$). (a) 27 years; (b) 158 years; (c) 318 years and (d) 438 years.

time. For large values of time, the degraded depth develops with the same $t^{1/2}$-kinetics (i.e. same slopes in Fig. 6), indicating that the degradation process at the fracture–matrix interface is governed by the 1D diffusive transport prevailing in the bulk material. From the $\sqrt{2b}$-dependence of the diffusion dominated mass transport in the fracture, it is readily understood that this switch occurs the earlier in time and the stronger, the smaller the fracture opening. Therefore, as expected from physical evidence, the smaller the fracture opening, the less affects a diffusion–dominated mass transport in the fracture the overall degradation process. The plots of solid calcium concentration displayed in Fig. 7 illustrate this limited effect of a fracture: for large times, the difference between the positions of the degradation fronts along the fracture and in the bulk material becomes constant.

3.3. Advection dominated mass transport in the fracture

The acceleration of the chemical degradation at the fracture–matrix interface due to advective mass transport is displayed in Fig. 8. Applying boundary condition $\mathscr{B}1$, the figure shows the fracture degradation

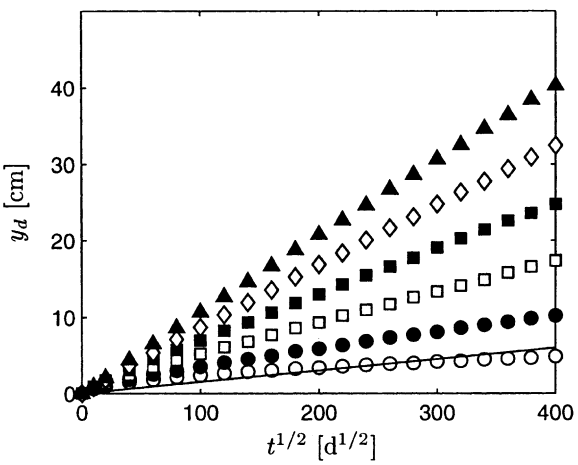

Fig. 8. Fracture degradation length y_d versus $t^{1/2}$ for advective and diffusive mass transport in the fracture, a zero solid matrix diffusivity in the y-direction, and a crack opening $2b = 0.2$ mm. Average fluid velocity V: (○) 0 cm/day; (●) 4 cm/day; (□) 8 cm/day; (■) 12 cm/day; (◇) 16 cm/day; (◆) 20 cm/day. The solid line corresponds to the 1D degradation of the solid matrix ($x_d = 1.5 \times 10^{-2}\sqrt{t}$ with t in days and x_d in cm) (boundary condition $\mathscr{B}1$).

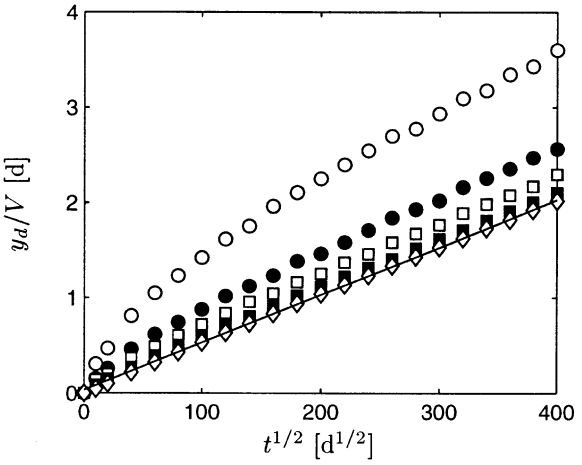

Fig. 9. Fracture degradation length y_d/V versus $t^{1/2}$ for advective and diffusive mass transport in the fracture of opening $2b = 0.2$ mm. Average fluid velocity V: (○) 2 cm/day; (●) 4 cm/day; (□) 6 cm/day; (■) 10 cm/day; (■) 20 cm/day. The solid line corresponds to the linear regression of the displayed (◇) data for times $t > 2$ years (boundary condition $\mathscr{B}1$).

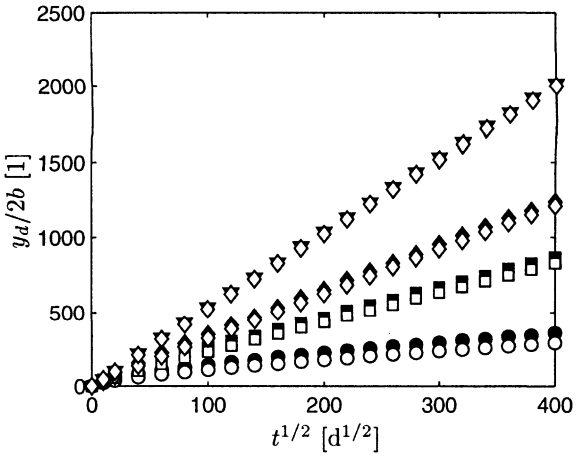

Fig. 10. Fracture degradation length $y_d/2b$ versus $t^{1/2}$ for advective and diffusive mass transport in the fracture for two crack openings. Black symbols correspond to a crack opening $2b = 0.2$ mm, and white symbols to $2b = 0.4$ mm. Average fluid velocity V: (○) and (●) 2 cm/day; (□) and (■) 8 cm/day; (◇) and (◆) 14 cm/day; (▽) and (▼) 20 cm/day (boundary condition $\mathscr{B}1$).

length $y_d(t)$ as a function of the square root of time for a fixed crack opening of $2b = 0.2$ mm, and fluid flow velocities ranging from $V = 2$ cm/d to $V = 20$ cm/d. To check the relevance of the asymptotic solution (24), Figs. 9 and 10 show the same results in a plot of $y_d(t)/V$ versus $t^{1/2}$, and $y_d(t)/2b$ versus $t^{1/2}$ for different crack openings. The results confirm the found asymptotic behavior (24):

- The degraded depth $y_d(t)$ is asymptotically a linear function of the square root of time for 'high' fluid velocities of $V \geqslant 8$ cm/d, corresponding roughly to a Péclet number on the order of $Pe \approx 80$ (with $L_y \simeq 18$ cm estimated from Fig. 8).

- As the velocity increases, the results in Fig. 9 converge to a straight line in a plot of y_d/V versus $t^{1/2}$, which represents the asymptotic solution (24).
- For different crack openings ($2b = 0.2$ mm and $2b = 0.4$ mm), the results in Fig. 10 perfectly align along straight lines in a plot of $y_d/2b$ versus $t^{1/2}$, as predicted by the asymptotic solution (24). By linear regression, the results displayed in Figs. 9 and 10 for high fluid velocities ($V \geqslant 10$ cm/d) can be expressed in the form:

$$\frac{y_d^{adv}(t)}{2bV} = 0.25\sqrt{t} + 1.71 \tag{31}$$

where y_d^{adv} and $2b$ are expressed in cm, the fluid velocity V in cm/d, and time t in days. Eq. (31) gives an upper bound for the evolution of the degradation process in the fracture in the case of advection mass transport in the fracture.

Finally, the solid straight line in Fig. 8 represents the 1D-dissolution process prevailing in the uncracked porous medium. In contrast to the diffusion dominated process (see Fig. 3), it appears that the 1D-diffusion–dissolution process is too slow to catch up with the faster degradation process along the fracture induced by advective mass transport. 'High' fluid flow velocities in a fracture, therefore, can induce a significant acceleration of the overall chemical degradation of the material. This acceleration can be depicted from Fig. 11 which shows the solid calcium concentration at different times for a fluid velocity of $V = 10$ cm/d and a crack opening of 0.4 mm.

Last, we should note that the dissolution process can become a rate limiting mass transport process for 'high' fluid velocity in the fracture, for which the dissolution kinetics can no more be considered as instantaneous with regard to the advection dominated mass transport. In this case, the dissolution kinetics in the vicinity of the fracture–matrix interface need to be taken into account.

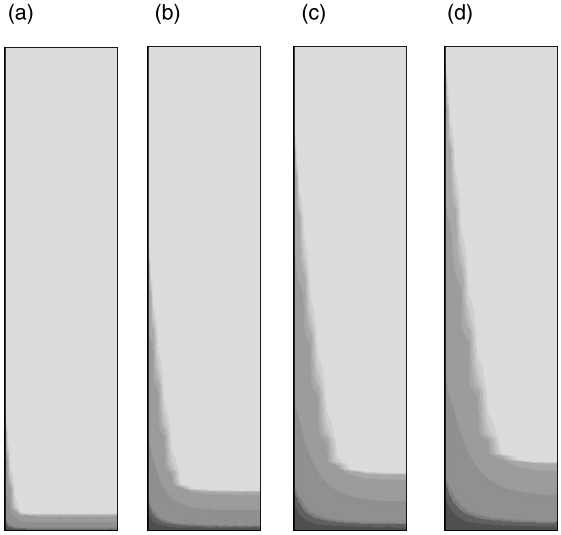

Fig. 11. Solid calcium concentration for an advective dominated mass transport in the fracture at different times (crack width $2b = 0.4$ mm; mesh $= 10 \times 50$ cm^2) (boundary condition $\mathscr{B}2$). (a) 27 years; (b) 158 years; (c) 318 years and (d) 438 years.

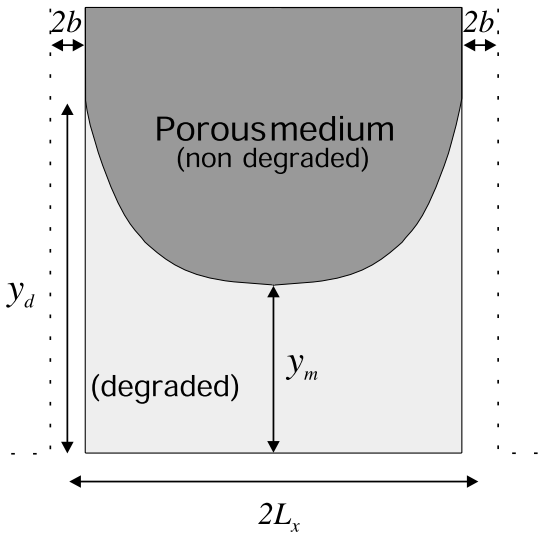

Fig. 12. Material degradation in case of a crack network of parallel fractures.

3.4. Effect of a fracture network

The last application we consider is the case of a crack network characterized by parallel fractures of same width $2b$ and equal spacing $2L_x$, as sketched in Fig. 12. This application represents a possible worst case scenario of multiple cracks that affect the chemical degradation process. Only the case of diffusion dominated mass transport in the fractures will be considered. Taken the symmetry of the regular crack spacing, the numerical simulations are realized on one half-part of the displayed geometry (i.e. $0 < x < L_x$, with $x = 0$ at the center of the fracture) with symmetrical boundary conditions at $x = 0$ and $x = L_x$, and a zero calcium concentration prescribed along $y = 0$ (i.e., boundary condition $\mathscr{B}2$).

Figs. 13 and 14 show the fracture degradation length y_d and the degradation length between two fractures y_m (see Fig. 12) as a function of the square root of time for a crack opening of $2b = 0.2$ mm, and different crack spacings $2L_x$. Both figures indicate:

- For large times, the degradation lengths y_d and y_m develop with the square root of time. For large crack spacings, the kinetics of the degradation follow the one of the 1D-dissolution process. In turn, the increasing slopes for small crack spacings in Figs. 13 and 14 indicate an acceleration of the overall degradation process.
- For a given crack opening $2b$ and crack spacing $2L_x$, the same asymptotic slope characterizes the degradation length kinetics at both the fracture matrix interface, i.e. y_d at $x = 0$, and between two fractures, i.e. y_m at $x = L_x$. This is shown in Fig. 15, and suggests the introduction of the crack spacing factor:

$$f = \frac{L_x}{b} \tag{32}$$

The crack spacing factor is obviously an invariant characterizing the chemical degradation kinetics. This can be depicted from Fig. 16 , which displays in the y_d versus $t^{1/2}$-plot the same asymptotic slopes for different crack openings $2b \in [0.1, 1]$ mm, having the same value of crack spacing factor $f = 40$. The increase in the $t^{1/2}$-slope for different crack spacing factors f is shown in Fig. 17, in which the slope of the asymptotic linear behavior is normalized by the slope of the 1D behavior (i.e. 1.5×10^{-2} cm/s$^{1/2}$). The

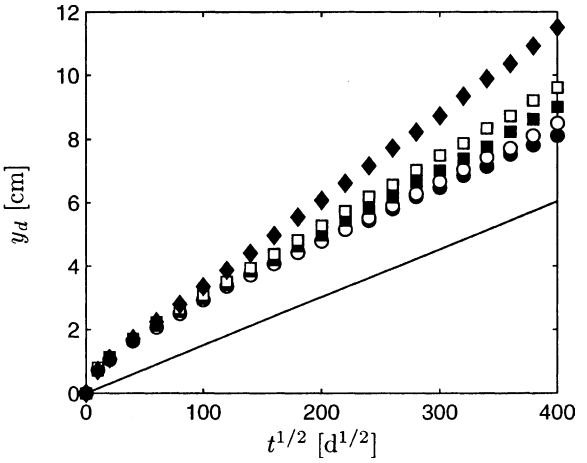

Fig. 13. Fracture degradation length y_d versus $t^{1/2}$ for $2b = 0.2$ mm, and different fracture spacing $2L_x$: (●) 20 cm; (○) 2 cm; (■) 1.2 cm; (□) 0.8 cm; (♦) 0.4 cm. The solid line corresponds to the 1D degradation ($x_d = 1.5 \times 10^{-2}\sqrt{t}$ with t in days and x_d in cm) (boundary condition $\mathscr{B}2$).

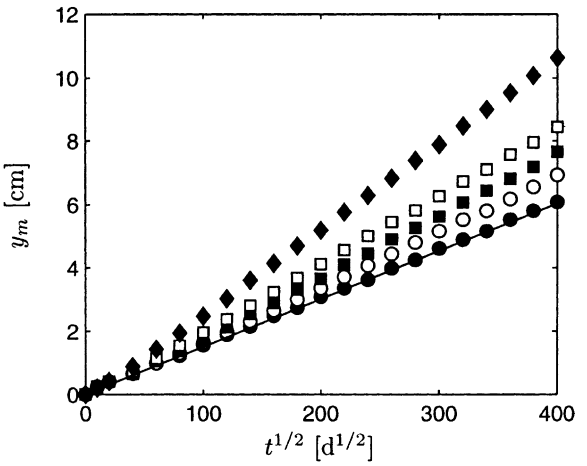

Fig. 14. Degradation length y_m between two fractures versus $t^{1/2}$ for $2b = 0.2$ mm, and different fracture spacing $2L_x$: (●) 20 cm; (○) 2 cm; (■) 1.2 cm; (□) 0.8 cm; (♦) 0.4 cm. The solid line corresponds to the 1D degradation ($x_d = 1.5 \times 10^{-2}\sqrt{t}$ with t in days and x_d in cm) (boundary condition $\mathscr{B}2$).

results confirm, that small values of the crack spacing factor lead to a high acceleration of the degradation kinetics, while the normalized slope function converges to unity for large values of f.

A first-order analysis of this behavior can be developed with the simplified single phase dissolution model presented in the first part of this paper. To this end, consider that the propagation of the dissolution front results from the mass transport in the y-direction in both the material and the fracture, with a dissolution front which propagates with the square root of time through the bulk material:

$$y_d(t) = \bar{y}_f\sqrt{D_m t} \tag{33}$$

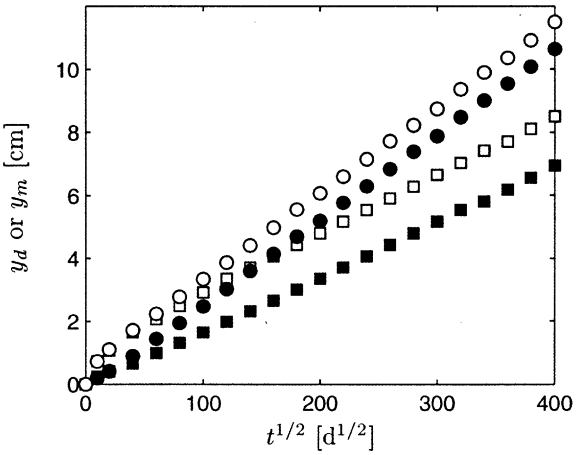

Fig. 15. Degradation lengths y_d (white symbols) and y_m (black symbols) versus $t^{1/2}$ for $2b = 0.2$ mm, and different fracture spacing $2L_x$: (●) and (○) 0.4 cm; (■) and (□) 2 cm (boundary condition $\mathscr{B}2$).

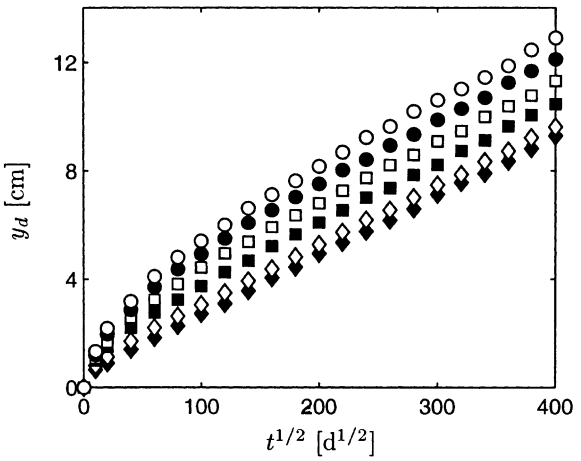

Fig. 16. Fracture degradation length y_d versus $t^{1/2}$ for two different crack openings, having the same crack spacing factor $f = 40$. $2b$: (○) 1 mm; (●) 0.8 mm; (□) 0.6 mm; (■) 0.4 mm; (◇) 0.2 mm; (◆) 0.1 mm (boundary condition $\mathscr{B}2$).

In Eq. (33), $\bar{y}_f$ is a function to be identified from the jump or Rankine–Hugoniot condition, which expresses the mass conservation across the dissolution front:

$$(L_x - b)m_0 \frac{\partial y_d}{\partial t} = (L_x - b)D_m \phi \frac{\partial \rho_m}{\partial y}|_{y=y_d(t)} + bD_f \frac{\partial \rho_f}{\partial y}|_{y=y_d(t)} \tag{34}$$

The left-hand side in Eq. (34) represents the rate of mineral mass which is dissolved by the moving dissolution front from $y_d(t)$ to $y_d(t + dt)$ between time t and $t + dt$. This mass rate is transported by diffusive flux in the solid material and the fracture away from the dissolution front. This is expressed by the right-hand side of Eq. (34). Furthermore, if we assume the macroscopic solubility $\varepsilon = \phi\rho_m/m_0$ much smaller than unity (i.e. $\varepsilon \ll 1$), the dissolution front will propagate slowly through the material, so that it is reasonable to

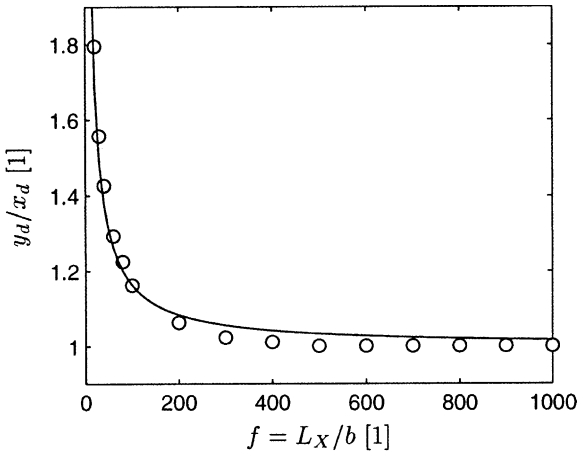

Fig. 17. Slope acceleration factor versus crack spacing factor f. The straight line corresponds to Eq. (37), with a value of $D_f/(\phi D_m) = 35$.

assume a linear spatial distribution of ρ_m and ρ_f in the y-direction between the boundary of the material and the dissolution front, i.e. in Eq. (34):

$$\frac{\partial \rho_m}{\partial y}|_{y=y_d(t)} \approx \frac{\rho_{eq}}{\bar{y}_f\sqrt{D_m t}}; \quad \frac{\partial \rho_f}{\partial y}|_{y=y_d(t)} \approx \frac{\rho_{eq}}{\bar{y}_f\sqrt{D_m t}}. \tag{35}$$

Then, substituting Eqs. (33) and (35) in Eq. (34), gives function $\bar{y}_f$, and the front position:

$$y_d(t) = \sqrt{2\varepsilon}\sqrt{1 + \frac{1}{f-1}\frac{D_f}{\phi D_m}}\sqrt{D_m t} \tag{36}$$

Note that the term $\sqrt{2\varepsilon}$ in Eq. (36) is a first order approximation of function $2\bar{x}_d(\varepsilon)$ in Eq. (20) for small values of ε. Finally, for small values of ε letting $x_d(t) = \sqrt{2\varepsilon}\sqrt{D_m t}$, from Eqs. (20) and (36) we obtain an analytical expression of the slope ratio displayed in Fig. 17:

$$\frac{y_d(t)}{x_d(t)} = \sqrt{1 + \frac{1}{f-1}\frac{D_f}{\phi D_m}} \tag{37}$$

The solid line in Fig. 17 which fits the numerical results of model based simulations is obtained with a diffusivity ratio of $D_f/(\phi D_m) = 35$. Taken the rough hypotheses required to derive Eq. (37), this fit provides a reasonable approximation for assessing the effect of a crack network on the overall degradation kinetics for large times.

4. Conclusion

The chemical degradation of cracked cement-based materials is governed by (i) mass transfer by dissolution from the material to the interstitial solution; (ii) molecular diffusion in the porous matrix; (iii) molecular diffusion and mechanical dispersion in cracks and fractures; and (iv) advection (or convection) in the fracture channel. Diffusion and advection in the fracture operate in opposite directions. Diffusion

evacuates calcium ions to the boundary, while advection imports the lower boundary condition into the fracture. This has the following consequences:

1. Diffusion dominated mass transfer in fractures does not significantly increase the material degradation. The propagation of the fracture degradation length develops with the quadratic root of time, until the faster $t^{1/2}$-front propagation through the bulk material catches up with the $t^{1/4}$-degradation process in the fracture. This shift in self-similarity occurs the earlier the smaller the fracture width, in cracked porous materials with fractures of aspect ratios $L_y/2b > 200$ (estimated from Eq. (30) and the solution of the 1D-calcium leaching process). For smaller fracture aspect ratio, a solute congestion will occur in the fracture: the diffusion in the fracture is too slow to evacuate the mineral dissolved in the adjacent porous materials to the outside.

2. Advection dominated mass transfer in fractures can significantly accelerate the overall calcium depletion in the porous materials for fluid velocities $V \geqslant 10$ cm/d. In this case, an upper bound assessment of the advection induced material degradation is provided by Eq. (31), which confirms the similarity properties of the asymptotic solution: a square-root of time dependence together with a linear dependence of the fracture degradation length on both velocity V and crack opening $2b$.

3. Diffusive dominated mass transport in a crack network may accelerate the calcium leaching process in porous materials. However, since the degradation induced through the fracture is restricted to small areas in the close vicinity of the fracture, the crack spacing must be sufficiently small to enhance the material degradation, i.e. typically for crack spacing factors $f = L_x/b \lesssim 100$. Eq. (37), derived from simplifying assumptions and validated through model-based simulations, provides a first order estimate of the effect of a crack network on the acceleration of the calcium degradation as a function of the crack spacing factor f and the ratio of the fracture and material diffusivities.

4. Temperature effects on the dissolution and transfer processes were not considered in this study. In concrete applications in nuclear waste disposal systems, temperature gradients with the surrounding environment may accelerate the material leaching and, more particularly, the mass transfer in the fracture. Similarly to the effect of the advective term in the solute conduction law, but less pronounced, these temperature gradients are expected to accelerate the overall chemical degradation process.

Acknowledgements

This research was performed as part of grant no. DE-FG03-99SF21891/A000 of the US Department of Energy (DOE) to MIT. The authors gratefully acknowledge the support of this work by the Nuclear Energy Research Initiative Program of DOE, and the collaboration with the Commissariat à l'Etude Atomique (CEA, Saclay, France), through Dr. Jérôme Sercombe. The numerical developments presented in this paper were realized within the finite element program CESAR-LCPC. The authors gratefully acknowledge the support by the service MPI of Laboratoire Centrale des Ponts et Chaussées, who provided the source files for the development in CESAR-LCPC@MIT.

References

Adenot, F., 1992. Durabilité du béton: caractérisation et modélisation des processus physiques et chimiques de dégradation du ciment. Ph.D. Thesis, Université d'Orléans, France (in French).

Adenot, F., Buil, M., 1992. Modelling of the corrosion of the cement paste by deionized water. Cement and Concrete Research 22, 489–496.

Aris, R., 1956. On the dispersion of a solute in a fluid flowing through a tube. Proceedings of the Royal Society of London, Ser. A 235, 67–77.

Bažant, Z.P., Şener, S., Kim, J.K., 1987. Effect of cracking on drying permeability and diffusivity of concrete. ACI Materials Journal 84, 351–357.

Bažant, Z.P., Raftshol, W.J., 1982. Effect of cracking in drying and shrinkage specimens. Cement and Concrete Research 12, 209–226.

Bear, J., 1991. Mathematical modelling of transport in porous media. In: Bear, J., Buchlin, J.M. (Eds.), Modelling and Applications of Transport Phenomena in Porous Media. Kluwer, Academic Publisher, Dordrecht.

Bear, J., 1993. Modeling flow and contaminant transport in fractured rocks. In: Bear, J, Tsang, C.-F., de Marsily, G. (Eds.), Flow and Contaminant Transport in Fractured Rock. Academic Press, New York.

Berner, U.R., 1988. Modelling the Incongruent Dissolution of Hydrated Cement Minerals. Radiochimica Acta 44/45, 387–393.

Berner, U.R., 1992. Evolution of pore water chemistry during degradation of cement in a radioactive waste repository environment. Waste Management 12, 201–219.

Buil, M., Revertegat, E., Oliver, J., 1992. A model of the attack of pure water or undersaturated lime solutions on cement. In: Gilliam, T.M., Wiles, C.C. (Eds.), Stabilisation and Solidification of Hazardeous, Radioactive, and Mixed Wastes, vol. 2, pp. 227–241.

Carslaw, H.S., Jaeger, J.C., 1959. Conduction of heat in solids, second ed. Oxford Science Publication, London.

Daïan, J.-F., Saliba, J., 1993. Transient moisture transport in a cracked porous media. Transport in Porous Media 13, 239–260.

Delagrave, A., Gérard, B., Marchand, J., 1997. Modelling the calcium leaching mechanisms in hydrated cement pastes. In: Scrivener, K.L., Young, S.F. (Eds.), Mechanisms of chemical degradation of cement-based systems. Proceedings of MRS Fall Meeting. E & FN Spon, London, pp. 38–49.

Gérard, B., Marchand, J., 2000. Influence of cracking on the diffusion properties of cement-based materials. Part I: Influence of continuous cracks on the steady-state regime. Cement and Concrete Research 30, 37–43.

Gérard, B., 1996. Contribution des couplages mécanique-chimie-transfert dans la tenue à long terme des ouvrages de stockage des déchets radioactifs. Ph.D. Thesis, ENS Cachan, France (in French).

Grisak, G.E., Pickens, J.F., 1980. Solute transport through fractured media. 1. The effect of Matrix Diffusion. Water Resources Research 16, 719–730.

Hughes, T.J.R., 1987. The finite element method. Linear Static and Dynamic Finite Element Analysis, second edn. Prentice-Hall, Englewood Cliffs, NJ.

Ippolito, I., Daccord, G., Hinch, E.J., Hulin, J.-P., 1994. Echo tracer dispersion in model fractures with a rectangular geometry. Journal of Contaminant Hydrology 16, 87–108.

Keer, J.G., Xu, G., Filip, R., 1989. Cracking and moisture penetration in fibre cement, sheeting. In: Swamy, R.N., Barr, B. (Eds.), Fibre Reinforced Cements and Concretes, Recent Developments. Elsevier, Amsterdam, pp. 592–601.

Lagoudas, D.C., Entchev, P., Triharjanto, R., 2000. Modeling of oxidation and its effect on crack growth in titanium alloys. Computer Methods in Applied Mechanics and Engineering 183, 35–50.

Lichtner, P.C., Oelkers, E.H., Helgeson, H.C., 1986. Exact and numerical solutions to the moving boundary problem resulting from reversible heterogeneous reactions and aqueous diffusion in a porous medium. Journal of Geophysical Research 91 (B7), 7531–7544.

Locoge, P., Massat, M., Ollivier, J.P., Richet, C., 1992. Ion diffusion in microcracked concrete. Cement and Concrete Research 22, 431–438.

Logan, J.D., Ledder, G., Homp, M.R., 1998. A singular perturbation problem in fractured media with parallel diffusion. Mathematical Models and Methods in Applied Sciences 8 (4), 645–655.

Mainguy, M., Coussy, O., 2000. Propagation fronts during calcium leaching and chloride penetration. Journal of Engineering Mechanics, ASCE 126 (3), 250–257.

Mainguy, M., Tognazzi, C., Torrenti, J.-M., Adenot, F., 2000. Modelling of leaching in pure cement paste and mortar. Cement and Concrete Research 30, 83–90.

Mainguy, M., Ulm, F.-J., 2000. Coupled diffusion–dissolution around a fracture channel: the solute congestion phenomenon, submitted for publication.

Martin, R., Burr, D., 1989. Structure, Function and Adaption of Compact Bone. Raven Press, New York.

Neretnieks, I., 1980. Diffusion in the rock matrix: an important factor in radionucleide retardation. Water Resources Research 85 (B8), 4379–4397.

Novak, C.F., 1993. Modeling mineral dissolution and precipitation in dual-porosity fracture–matrix systems. Journal of Contaminant Hydrology 13, 91–115.

Pettersson, K., Jørgensen, O., Fidjestøl, P., 1996. The effect of cracks on reinforcement concrete in a marine environment. In: Malhotra, V.M. (Ed.), Concrete in Marine Environment, Proceedings of the Third CANMET/ACI International Conference. Canada, pp. 185–191.

Rao, V.S., Hughes, T.J.R., 2000. On modelling thermal oxidation of silicon I: Theory. International Journal for Numerical Methods in Engineering 47, 341–358.

Reardon, E.J., 1992. Problems and approaches to the prediction of the chemical composition in cement/water systems. Waste Management 12, 221–239.

Samaha, H.R., Hover, K.C., 1992. Influence of microcracking on the mass transport properties of concrete. ACI Materials Journal 89 (4), 416–424.

Savage, D., Rochelle, C.A., 1993. Modelling reactions between cement pore fluids and rock: implications for porosity change. Journal of Contaminant Hydrology 13, 365–378.

Schiessl, P., Raupach, M., 1997. Laboratory studies and calculations on the influence of crack width on chloride-induced corrosion of steel in concrete. ACI Materials Journal 94 (1), 56–62.

Steefel, C.I., Lichtner, P.C., 1994. Diffusion and reaction in matrix bordering a hyperalkaline fluid-filled fracture. Geochimica et Cosmochimica Acta 58 (17), 3595–3612.

Sun, N.-Z., 1996. Mathematical Modeling of Ground water Pollution. Springer, Berlin.

Tang, D.H., Frind, E.O., Sudicky, E.A., 1981. Contaminant transport in fractured porous media: analytical solution for a single fracture. Water Resources Research 17 (3), 555–564.

Taylor, G.I., 1953. Dispersion of a soluble matter in solvent flowing slowly through a tube. Proceedings of the Royal Society of London Ser. A 219, 186–203.

Tognazzi, C., 1998. Couplage fissuration-dégradation chimique dans les matériaux cimentaires: caractérisation et modélisation. Ph.D. Thesis, INSA Toulouse, France (in French).

Torrenti, J.-M., Didry, O., Ollivier, J.-P., Plas, F. (Eds.), 1999. La dégradation des bétons. Couplage fissuration-dégradation chimique. Hermès, Paris (in French).

Ulm, F.-J., Torrenti, J.-M., Adenot, F., 1999. Chemoporoplasticity of calcium leaching in concrete. Journal of Engineering Mechanics ASCE 125 (10), 1200–1211.

Walton, J.C., Seitz, R.R., 1992. Fluid flow through fractures in below ground concrete vaults. Waste Management 12, 179–187.